Dynamics of ultrafast laser plasma expansion in the presence of an ambient

N. Farid,[1,2] S. S. Harilal,[1] H. Ding,[2] and A. Hassanein[1]
[1]*Center for Materials Under Extreme Environment, School of Nuclear Engineering, Purdue University, West Lafayette, Indiana 47907, USA*
[2]*Key Laboratory of Materials Modification by Laser, Ion and Electron Beams, School of Physics and Optical Engineering, Dalian University of Technology, Dalian, China*

(Received 18 July 2013; accepted 26 October 2013; published online 6 November 2013)

We investigated the role of ambient gas pressure on the expansion and the emission features during ultrafast laser ablation of metal target. Plasma plumes were generated using 800 nm, 40 fs laser pulses on a copper target and the ambient air pressure was varied more than seven orders (1×10^{-5} – 760 Torr) of magnitude. Fast-gated images showed a complex interaction between the plume and ambient leading to changes in the plume geometry with pressure as well as time. The ambient pressure levels are found to affect both the line intensities and broadening along with signal to noise (S/N) and signal to background (S/B) ratios. The optimum pressure condition for analytical applications is found to be ~100 Torr. © *2013 AIP Publishing LLC*. [http://dx.doi.org/10.1063/1.4829487]

Laser ablation (LA) has widespread applications and some of the prominent applications in the fields of material science and detection are pulsed laser deposition (PLD),[1] laser-ablation inductively coupled-plasma mass spectrometry (LA-ICP-MS),[2] nano-particles generation,[3] and laser induced breakdown spectroscopy (LIBS).[4] Typically laser ablation plumes expand adiabatically (free expansion) in vacuum and the presence of ambient gas not only affects its expansion dynamics but emission features as well. For example, previous studies employing nanosecond laser ablation at varying ambient pressures showed complex and violent interaction between the expanding plasma plumes and ambient leading to generation of shockwaves, plume splitting, instabilities, confinement, and creation of ambient plasma.[5–7] Ambient gases are routinely used in laser ablation applications for various purposes. For example, in PLD the ambient gas serves as a moderator for ions or for reactive scattering.[1] In LA-ICP-MS, the gas cools the ablation plumes rapidly leading to aerosol formation and flushes the aerosols to ICP torch.[2] In LIBS, the background gas confines the plasma leading to more excitation and emission. In laser absorption spectroscopy (LAS), the ambient gas species make the plume more collisional leading to increased S/N ratio.[8]

Recent advancements in ultrafast lasers opened up a new field of research named ultrafast laser ablation (ULA). The ULA has superior properties and advantages compared to nanosecond LA in many applications including reduced elemental fractionation in LA-ICP-MS,[9,10] precise micromachining,[11] reduced continuum emission in LIBS,[12] less droplets in PLD,[13] etc. The heat affected zone (HAZ) and material collateral damages were found be lesser for ULA compared to traditional long-pulse laser ablation since the pulse width of the fs laser is significantly shorter than the typical characteristic relaxation times (electron-ion, electron-lattice).[14] Even though the applications of ULA are ever growing, a study of the role of ambient gas on plume kinetics is still lacking. Considering highly transient nature of the laser ablation plumes, both in space and time, studying the plasma expansion dynamics and kinetics in the presence of an ambient is ultimately essential for most of the applications. In this letter, we report a comprehensive picture of dynamics of ultrafast laser ablation plumes in the presence of an ambient. Our studies showed a complex picture of plume interaction with ambient at different pressure levels. Emission analysis showed that the moderate pressure levels are the optimal conditions for obtaining the optimum of the S/N and S/B ratios.

The details of the experimental set up are given elsewhere.[15,16] Briefly, a copper (Cu) target with 2 mm thickness with a purity of 99.95% was used as the target material and positioned inside a vacuum chamber. The target was placed on a XY translational stage, which provided fresh surface for each laser shot exposure in order to avoid the crater formation. An ultrafast fs laser with 4.5 mJ at 40 fs pulse duration at full width at half-maximum (FWHM) was used for ablating the Cu target and generating plasma. Laser beam was focused perpendicular to the sample surface using a plano-convex lens (f = 40 cm) to a spot size ~300 μm leading to a laser irradiance at the target surface $\sim 3.5 \times 10^{14}$ Wcm^{-2}. The pressure of the ambient gas was varied by inserting air in the vacuum chamber through a leak valve. The time resolved plume expansion in vacuum and at different background pressure levels was studied using an intensified CCD (ICCD) camera (PI-MAX). The minimum gate time of intensifier was ~2 ns. For performing optical emission spectroscopy, the expanding plasma was collected in a direction normal to the plume expansion and imaged to entrance slit of a 0.75 m triple grating (3600, 1200, and 150 lines/mm) spectrograph (Andor). An Andor ICCD (iStar) was used as a detector for recording the dispersed spectra from the spectrograph.

Gated imaging employing ICCD is one of the best and easiest techniques for investigating the hydrodynamics of the plasmas as it provides a comprehensive picture of plume expansion and evolution.[6] Figure 1 gives the spectrally integrated plume images recorded at different time delays after the plasma onset, and at different background pressures of air (from vacuum to atmospheric pressure). Each image is normalized to its own maximum intensity for better view. In vacuum, the images show that the plume in cylindrical shape expands freely and rapidly in the forward direction. The

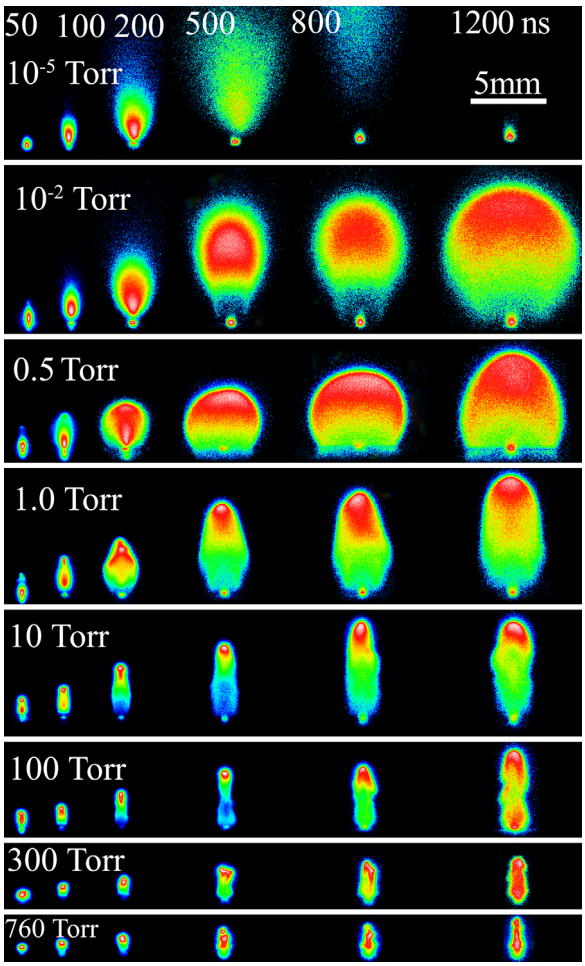

FIG. 1. Spectrally integrated and time resolved images of ultrafast laser ablation of Cu obtained using an ICCD camera. All the images were normalized to its maximum intensity for better view and captured using a gate width that corresponds to 10% of delay time. 800 nm, 4.5 mJ pulses were used for ablation with an intensity at the target $\sim 3.5 \times 10^{14}$ W/cm^2.

emission from the plasma is almost disappeared after ~800 ns delay and only the black body emission from nano particles can be seen in front of target surface at later times.[3] The preferential cylindrical expansion of fs LA in the normal direction can be understood by considering narrow cone ion emission.[17] The interaction between the plasma species and ambient gas species is found to be minimal when the pressure $\leq$1 mTorr. With increasing pressure, the plume gets brighter because of collisional excitation by ambient gas species. At a pressure of 1×10^{-2} Torr and for times $<$200 ns delay times, the plume propagation seems to be quite similar to that in vacuum. However, at later times, the plume geometry changes from the cylindrical to the spherical and persists for longer times. This was evidenced by the estimated aspect ratios at various times: 3 and 1 at times 100 ns and 1200 ns, respectively. At this pressure levels, the confinement of the plume happens at later times when the pressure exerted by the ambient gas is comparable with plume pressure. The confinement of plume will lead to enhanced collision resulting into recombination and higher persistence of all species in the plume. Similar confinement and changing of aspect ratio of the plasma plume has also been observed recently with the nano joule fs laser ablation.[18]

At higher pressure levels, e.g., 0.5 Torr, the plume geometry changes from cylindrical to spherical at earlier times ~100 ns. At 1 Torr pressure, the images show that the pressure exerted by the background fluid is higher, and the ambient gas drag affecting the plume both in the radial and in the axial directions generates a cylindrical plume during its entire lifecycle.

Compared to ns LA, most of the ions as well as ablated mass are ejected from target surface in a narrow cone angle with respect to the target normal for fs LA.[17] It has been reported that for the fs LA, the angular distribution of KE as well as the ion flux is about 3 times narrower than that for the nanosecond LA.[17] This results in cylindrical geometry for fs LA plumes at higher pressures due to the confinement. The plume splitting, a peculiar feature observed in the presence of an ambient gas, can also be seen at early time (~50 ns) for 1 and 10 Torr pressure levels which consists of fast and slow moving plume components. This effect is similar to that have been reported for ns LA[19] and explained due to fast moving highly ionized species at the plume front which detached from the slow moving component which essentially consists of lower velocity species. At higher-pressure levels ($\geq$100 Torr), the plume compressed by the background gas both in the radial as well as in the forward direction, the energetic species in the plume tend to succeed the confined region through a diffusion-like propagation.

Plume front position–delay time (R-t) plots were obtained from ICCD images, which are useful for obtaining better insights of plasma expansion dynamics at various ambient pressure levels. The R-t plots obtained with various ambient pressures as well as in vacuum are shown in the Fig. 2. At a 10^{-5} Torr, the plume front position followed a linear expansion with time indicating free expansion. However, at 1, 100, 300, and 760 Torr pressure levels, the plume expansion is described by the drag model which is given by $R = R_O(1-\exp(-\beta t))$, where R_0 is the stopping distance of the plume and β is the deceleration coefficient ($R_o\beta = v_o$). The

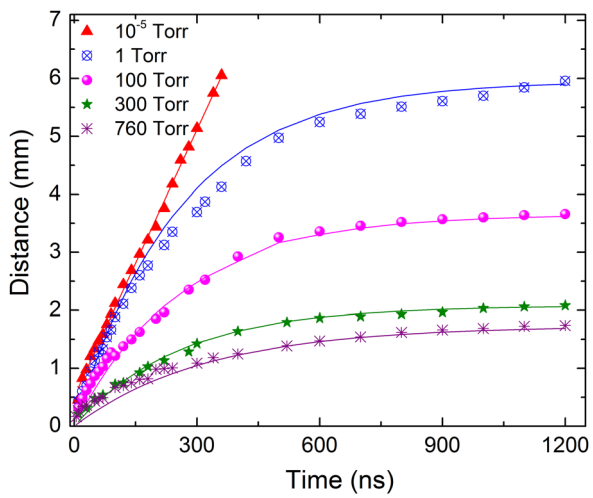

FIG. 2. R-t plots obtained from ICCD images are given for various pressure levels. The symbols in the figure represent experimental data points and curves represent linear, and drag model fitting for 10^{-5} and 1, 100, 300, and 760 Torr, respectively. The drag model fitting parameters are $\beta = 0.0039$ ns^{-1} and $R_O = 5.96$ mm (1.0 Torr), $\beta = 0.0038$ ns^{-1} and $R_O = 3.7$ mm (100 Torr), $\beta = 0.00324$ ns^{-1} and $R_O = 2.1$ mm (300 Torr) and for 760 Torr are $R_O = 1.8$ mm and $\beta = 0.0031$ ns^{-1}.

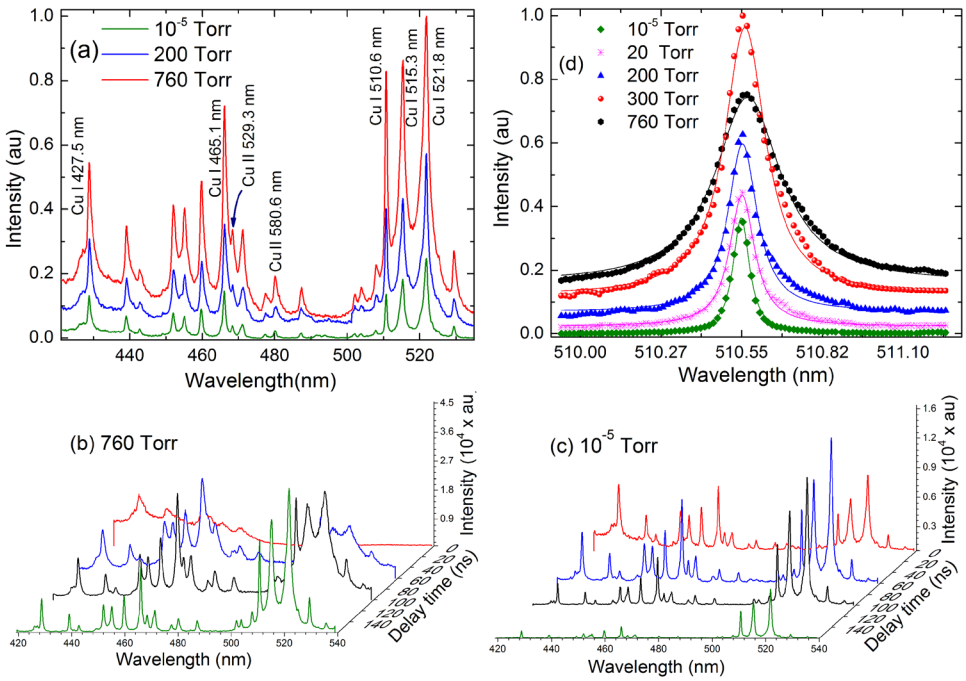

FIG. 3. (a) Representative emission spectra of fs laser-produced Cu plasma different at ambient pressure levels are given. The spectra were acquired after 100 ns delay and with 1 μs gate width. The time resolved emission features at (b) 760 Torr air and at (c) 10^{-5} Torr are given. A gate width of 10% of the delay time was used for the time resolved study. (d) Variation in line broadening with various pressure levels are given for Cu I (510.6 nm). The experimental data points are represented by symbols while solid lines represent the Lorentzian fitting.

deceleration coefficient changed from 0.0039 to 0.0031 ns^{-1} as the pressure increased from 1 to 760 Torr.

Figures 3(a)–3(c) show typical time integrated and resolved spectra recorded at various pressure levels. Figure 3(a) shows that the fs LPP spectra are dominated by excited neutrals. For fs laser ablation, the Coulomb explosion, phase explosion fragmentation processes, and thermal vaporization are the main mechanisms responsible for the ablation. The Coulomb explosion is the leading mechanism, which occurs near to the ablation threshold.[20] However, at higher laser intensities, phase explosion is followed by thermal vaporization of the bulk material, which occurs several picoseconds later. In phase explosion, ultrafast heating produces a temperature higher than the boiling point at a given pressure near the critical temperature.[21,22] Thermal vaporization is responsible for the generation of neutrals within the plume, as the most of species emit near the vaporization temperature of the target material and hence produces mostly neutral atomic species. The spectra recorded at atmosphere pressure showed a significant background continuum (Fig. 3(b)) while this continuum is considerably decreased with the reduction of ambient pressure (Fig. 3(c)). The spectral emission is also broadened with increasing pressure as shown in Fig. 3(d).

For analytical applications of fs LA, e.g., LIBS, the precision and detection limits are mainly depended on the signal to background (S/B) as well as signal to noise (S/N) ratios and background gas pressure levels significantly affect both these parameters. In general, the nature and pressure of the background gas control the characteristic line emission intensity, line width, continuum, and noise levels. Therefore, for analytical applications the studies of these parameters are very important. Figures 4(a) and 4(b) present the variation in the S/B and S/N as a function of background pressures at various delay times. A characteristic line of Cu I at 510.5 nm was used for investigating the S/B and S/N values. The signal is defined as the peak value minus the background whereas the noise is taken as the three times the standard deviation (3σ) in a 1 nm region of spectrum where emission line does not exist.[23]

As Fig. 4 shows, when the pressure decreases from 1 atmosphere, both S/B and S/N ratios increase steadily and attain a maximum value, and then decrease with reduction in pressure. The optimum S/B was observed at a pressure of ~50 Torr and at a delay time of 150 ns. The S/B ratio is found to be lower for shorter time delays because of the presence of strong continuum at earlier times (see Fig. 3). For example, the optimum S/B ratio is lowered by a factor of 2 when the delay time is reduced from 150 ns to 100 ns and this reduction is substantial at shorter time delays ($\leq$50 ns). The line intensities as well as the continuum background intensities

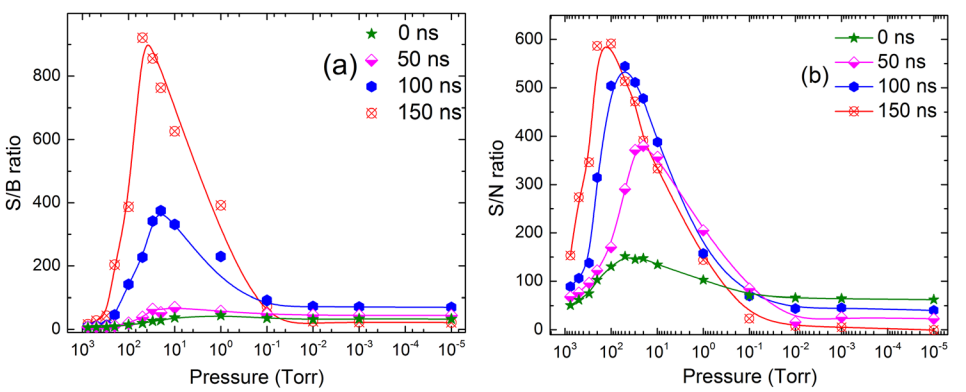

FIG. 4. The estimated S/B and S/N ratios are given as a function of background air pressure and delay times. The emission intensity of Cu I at 510.5 nm is used for estimating S/B and S/N ratios. Cu plasma was produced by fs laser pulses with 4.5 mJ energy and a 1 μs gate width was used for recording the spectra at various delay times.

increased with a rise in background pressure (Fig. 3(a)). Hence at higher pressure levels, although the line emission was relatively higher than at low pressures, the presence of larger background continuum tend to decrease the S/B ratio. The S/N ratios showed optimal conditions ~100 Torr at 150 ns delay and the optimal pressure levels decreased with reduction in delay times as shown in Fig. 4(b).

The S/N and S/B ratios showed optimal conditions in the pressure range ~50-100 Torr and they varied slightly depending upon the time of spectral capture. Images showed that the plume is approximately cylindrical during its entire lifetime at this pressure levels. The changes in signal intensity, noise level as well as the broadening of the line could be related to plasma confinement as seen in the fast gated images (Fig. 1) and changes in the fundamental parameters of the plasma, viz., temperature and density. Hence, we estimated the temperature and density of the plasma using spectroscopic means. Stark broadening and Boltzmann methods were employed for obtaining these parameters and details are given in Ref. 24. The variation of temperature and electron density as a function of pressure is given in Fig. 5. This measurement was done at 1 mm from the target with an integration time of 1 μs. The temperature variation trend is similar to S/N and S/B. As the pressure decreases from atmospheric levels, the temperature is found to increase and attain a maximum value at a pressure level ~100 Torr and then temperature decreases with further reduction in pressure. The increase in temperature of the plume from vacuum level to ~100 Torr can be related to plasma confinement and heating. At higher pressures, the reduction in temperature could be due to increased recombination, and cooling compensates the heating caused by the plasma confinement. Unlike temperature, the density curve showed decreasing values with lowering pressures. In order to evaluate the pressure effects on the broadening of emission lines, a Lorentz function was employed to fit the emission lines (see Fig. 3(d)). The narrowing of the Cu I 510.5 nm emission line was observed with decreasing pressure and is explained by the lowering of electron density of the plasma. A comparison of broadening with pressure shows that the lower pressure is better for getting well-resolved emission line. The electron density follows approximately $P^{0.34}$ dependence with pressure.

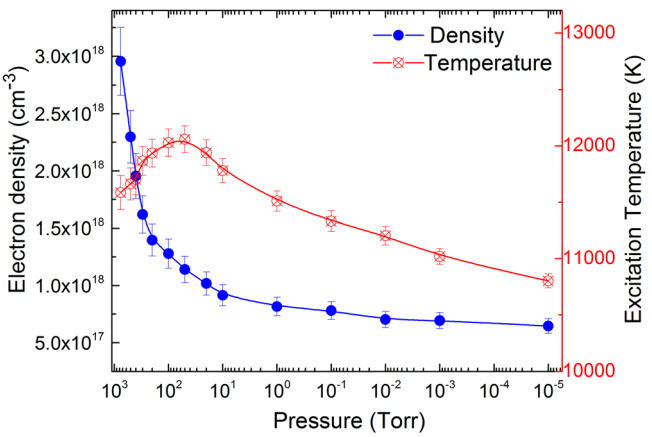

FIG. 5. The influence of background air pressure on electron density and temperature of Cu plasma is given. The electron density is decreased with pressure and followed a $P^{0.34}$ dependence. A characteristic line of Cu at 510.5 nm was used to determine the density while the temperature was measured by using Boltzmann's plots employing 427, 465, 510, 515, and 521 nm emission lines. Cu plasma was produced with a 4.5 mJ pulse energy and emission was acquired using a 1 μs gate width and 100 ns delay.

In conclusion, we report the role of ambient gas pressure on the expansion and the emission features of ultrafast laser ablation plumes from a metal target. The ambient pressure is found to greatly influence the shape, size and hydrodynamic expansion features of fs LA plumes along with line emission features, S/N and S/B ratios. Fast gated images employing ICCD showed a complex interaction between the plume and ambient leading to changes in the plume geometry with pressure as well as time. In vacuum as well as at higher pressure ambient levels, the fs LA plumes showed a cylindrical geometry while at moderate pressure levels the plume followed a spherical expansion geometry especially at later times. The ambient gas helps the plume to confine both in radial and axial directions leading to enhancement in both the line and background continuum emission intensities. But at higher pressure levels the emission analytical merit is reduced due to enhanced continuum. The spectral lines are broadened with increasing the pressure. The optimum emission S/N and S/B are obtained at a pressure level of ~100 Torr and it strongly depended on time window of spectral acquirement. The S/N ratio trend is found to follow approximately the temperature of the plasma plume.

This work was partially supported by the US DOE, Office of National Nuclear Security Administration under Award No. DE-NA0001174.

[1]D. B. Chrisey and G. K. Hubler, *Pulsed Laser Deposition of Thin Films* (John Wiley & Sons Australia, Limited, 1994).
[2]N. L. LaHaye, S. S. Harilal, P. K. Diwakar, A. Hassanein, and P. Kulkarni, J. Appl. Phys. **114**, 023103 (2013).
[3]S. Amoruso, R. Bruzzese, N. Spinelli, R. Velotta, M. Vitiello, X. Wang, G. Ausanio, V. Iannotti, and L. Lanotte, Appl. Phys. Lett. **84**, 4502 (2004).
[4]D. A. Cremers and L. J. Radziemski, *Handbook of Laser-Induced Breakdown Spectroscopy* (Wiley, 2006).
[5]S. S. Harilal, B. O'Shay, Y. Z. Tao, and M. S. Tillack, J. Appl. Phys. **99**, 083303 (2006).
[6]S. S. Harilal, C. V. Bindhu, M. S. Tillack, F. Najmabadi, and A. C. Gaeris, J. Appl. Phys. **93**, 2380 (2003).
[7]F. Nazar, S. S. Harilal, H. Ding, and A. Hassanein, Phys. Plasmas **20**, 073114 (2013).
[8]N. Taylor and M. C. Phillips, *Measurements of Uranium Line Widths and Pressure Broadening Coefficients in Atmospheric Pressure Laser-Induced Plasmas*, OSA Tech. Dig. 2013, CTu2H.2.
[9]R. E. Russo, X. L. Mao, J. J. Gonzalez, and S. S. Mao, J. Anal. At. Spectrom. **17**, 1072 (2002).
[10]P. K. Diwakar, S. S. Harilal, N. L. LaHaye, A. Hassanein, and P. Kulkarni, J. Anal. At. Spectrom. **28**, 1420 (2013).
[11]M. Q. Ye and C. P. Grigoropoulos, J. Appl. Phys. **89**, 5183 (2001).
[12]J. R. Freeman, S. S. Harilal, P. K. Diwakar, B. Verhoff, and A. Hassanein, Spectrochim. Acta, Part B **87**, 43 (2013).
[13]O. Albert, S. Roger, Y. Glinec, J. C. Loulergue, J. Etchepare, C. Boulmer-Leborgne, J. Perriere, and E. Millon, Appl. Phys. A: Mater. Sci. Process. **76**, 319 (2003).
[14]R. Le Harzic, N. Huot, E. Audouard, C. Jonin, P. Laporte, S. Valette, A. Fraczkiewicz, and R. Fortunier, Appl. Phys. Lett. **80**, 3886 (2002).
[15]K. F. Al-Shboul, S. S. Harilal, and A. Hassanein, Appl. Phys. Lett. **100**, 221106 (2012).
[16]K. F. Al-Shboul, S. S. Harilal, and A. Hassanein, J. Appl. Phys. **113**, 163305 (2013).
[17]B. Verhoff, S. S. Harilal, and A. Hassanein, J. Appl. Phys. **111**, 123304 (2012).

[18]S. P. Banerjee, Z. Chen, and R. Fedosejevs, J. Appl. Phys. **113**, 183101 (2013).
[19]S. S. Harilal, C. V. Bindhu, M. S. Tillack, F. Najmabadi, and A. C. Gaeris, J. Phys. D: Appl. Phys. **35**, 2935 (2002).
[20]H. Dachraoui and W. Husinsky, Appl. Phys. Lett. **89**, 104102 (2006).
[21]P. Lorazo, L. J. Lewis, and M. Meunier, Phys. Rev. Lett. **91**, 225502 (2003).
[22]N. M. Bulgakova and I. M. Bourakov, Appl. Surf. Sci. 197–198, **41** (2002).
[23]R. Noll, Anal. Bioanal. Chem. **385**, 214 (2006).
[24]N. Farid, C. Li, H. Wang, and H. Ding, J. Nucl. Mater. **433**, 80 (2013).